


Macroporous hydrogels derived from aqueous dynamic phase separation

Journal Article

Author(s):

Brogiere, Nicolas; Husch, Andreas; Palazzolo, Gemma; Bradke, Frank; Madduri, Srinivas; [Zenobi-Wong, Marcy](#) 

Publication date:

2019-04

Permanent link:

<https://doi.org/10.3929/ethz-b-000325948>

Rights / license:

[In Copyright - Non-Commercial Use Permitted](#)

Originally published in:

Biomaterials 200, <https://doi.org/10.1016/j.biomaterials.2019.01.047>

Funding acknowledgement:

166052 - Chondrogenic Bioinks for Bioprinting Stable Cartilage Grafts (SNF)

SLB 03.09.19-06.06 - Lattice Light Sheet Mikroskops für ScopeM (ETHZ)

Macroporous Hydrogels Derived from Aqueous Dynamic Phase Separation

*Nicolas Broguiere, Andreas Husch, Gemma Palazzolo, Frank Bradke, Srinivas Madduri, Marcy Zenobi-Wong**

N. Broguiere, Dr. G. Palazzolo, Prof. M. Zenobi-Wong

Tissue Engineering and Biofabrication Laboratory, Department of Health Sciences and Technology, ETH Zürich, Otto-Stern-Weg 7, 8093 Zürich, Switzerland.

Dr. A. Husch, Prof. F. Bradke,

Axon Growth and Regeneration Laboratory, German Center for Neurodegenerative Diseases, Sigmund-Freud-Str. 27, 53127 Bonn.

Dr. S. Madduri

Center for Bioengineering and Regenerative Medicine, Department of Biomedical Engineering, University of Basel, Gewerbestrasse-14, 4123 Allschwil
Department of Biomedicine, University of Basel, Hebelstrasse 20, 4031 Basel
Department of Plastic, Reconstructive, Aesthetic and Hand Surgery, University Hospital Basel, Klinikum 1, Spitalstrasse 21, 4031 Basel.

*Corresponding author:

Prof Marcy Zenobi-Wong, Tissue Engineering and Biofabrication laboratory, HPL J20, Otto-Stern-Weg 7, 8093 Zürich, Switzerland

E-mail: marcy.zenobi@hest.ethz.ch

Abstract: A method to generate injectable macroporous hydrogels based on partitioning of polyethylene glycol (PEG) and high viscous polysaccharides is presented. Step growth polymerization of PEG was used to initiate a phase separation and the formation of a connected macroporous network with tunable dimensions. The possibilities and physical properties of this new category of materials were examined, and then applied to address some challenges in neural engineering. First, non-degradable macroporous gels were shown to support rapid neurite extension from encapsulated dorsal root ganglia (DRGs) with unprecedented long-term stability. Then, dissociated primary rat cortical neurons could be encapsulated with >95% viability, and extended neurites at the fast rate of $\approx 100 \mu\text{m}/\text{day}$ and formed synapses, resulting in functional, highly viable and long-term stable 3D neural networks in the synthetic extracellular matrix (ECM). Adhesion cues were found unnecessary provided the gels have optimal physical properties. Normal electrophysiological properties were confirmed on 3D cultured mouse hippocampal neurons. Finally, the macroporous gels supported axonal growth in a rat sciatic nerve injury model when used as a conduit filling.

The combination of injectability, tunable pore size, stability, connectivity, transparency, cytocompatibility and biocompatibility, makes this new class of materials attractive for a wide range of applications.

Keywords: macroporous, hydrogel, neuron, tissue, engineering, microstructures, porous, materials, biomimetics, biomedical, bioengineering, neural, networks, nerve

1. Introduction

Most neurons can quickly extend neurites and form active networks when encapsulated in natural ECM components such as fibrin, collagen, or laminin [1–3]. These ECM proteins have coevolved together with the neurons to provide optimal pore size, stiffness and adhesion. They nevertheless have limitations: the adhesion and degradation are not easily tunable, they can trigger immune reactions when used in vivo (e.g. matrigel is produced by mouse tumors and immunogenic to humans), they typically degrade too fast and are poorly characterized with batch to batch variations. Further disadvantages include the risk of disease transmission and the high cost of isolation from animal tissue/blood or recombinant protein production. Analogous to the shift away from serum containing media to defined media, there is current interest to move from animal-derived ECMs to defined synthetic ECMs. Such artificial ECMs could find applications as 3D cell culture models in vitro and for in vivo tissue regeneration[4–6] or as a vehicle for cells, enzymes, and growth factors [7,8].

PEG hydrogels have proven to be one of the most versatile artificial ECM systems [9,10]. Being very weakly interactive with biological systems, PEG hydrogels represent an ideal “blank” 3D matrix in which the bioactivity of molecules can be studied [11]. This weak interactivity also leads to reduced toxicity and/or immunogenicity [12], and PEG has been approved by the US Food and Drug Administration (FDA) for various clinical applications. PEG is often used as a stealth or anti-adhesive material [13–15], and PEG gels were shown to be biocompatible in rat [16] and primate [17] brains upon implantation. A heparin-PEG copolymer hydrogel was also recently shown to support 3D cultures of various primary and human neural progenitor cells, and could be used as a functional model for Alzheimer’s disease [18]. Nevertheless, a hydrogel with pure PEG backbone that promotes formation of 3D electrically-active neural networks from primary cultures through high viability, fast neurite outgrowth and synapse formation has not yet been achieved. Dissociated neurons are particularly challenging because, unlike neurons grown as a sphere or cluster, they are maximally exposed to environmental stresses such as toxic chemicals, and lack the contact adhesion, ECM and high local levels of enzymes and growth factors secreted by neighboring cells. In the current state of the art, neurite extension from neural clusters was seen in PEG gels but only at a late stage of gel degradation [19]. Non-degradable gels optimized for 2D culture of neural progenitor cells were found to be non-permissive to 3D growth [20]. Using fibrin inclusion and degradation to make PEG gels porous, still very little neurite outgrowth was observed after 13 days of culture [21]. The method of Hubbell and coworkers using matrix metalloproteinase (MMP)-sensitive peptides to impart cell-mediated biodegradability to PEG hydrogels [22] has been successful for multiple cell types, but when applied to

neurons, this method gave viabilities of 4 to 21% and limited neurite outgrowth [23]. More generally, it has been a challenge to optimize synthetic matrices for dissociated neurons not only because of their sensitivity to the chemical stress associated with encapsulation, but also because the extremely soft materials that support fast neurite extension are short lived, whereas stronger, biostable materials are poorly permissive.

We present a protocol which demonstrates an unprecedented combination of 3D neurite outgrowth and stability in the presence of encapsulated DRGs and primary hippocampal and cortical neurons based on the formation of an interconnected macroporous network. The key to our protocol is the use of non-modified high molecular weight polysaccharides for PEG exclusion (hyaluronan (HA) or the non-interactive mannuronan (MA), eventually in combination with dextran to increase pore size of the network). Exclusion of PEG from the polysaccharide phase improves the kinetics of the cross-linking by Michael addition of thiols on vinyl sulfones (VS), so that gelation proceeds within minutes in media at physiological pH, instead of requiring pH 8.0 which is damaging to sensitive cells such as neurons. The phase separation between the PEG and polysaccharides also results in gels with increased stability and neurite outgrowth compared to the non-microstructured versions. Adhesion cues such as proteins or integrin binding peptides are unnecessary in our system, exemplifying the overwhelming importance of physical properties in engineering a neurite permissive ECM.

In optimized conditions, encapsulated hippocampal/cortical neurons extended neurites at a typical rate of 100 $\mu\text{m}/\text{neuron}/\text{day}$ and formed synapses in our synthetic matrix, which resulted in 3D neural networks with spontaneous coordinated electrical activity after two weeks, remaining stable for at least a month in culture.

Other methods have been described to generate injectable macroporous hydrogels. For example, a combination of ammonium persulfate, ascorbic acid and sodium bicarbonate could be used to evolve carbon dioxide, while polymerizing propylene fumarate-*co*-ethylene glycol [24]. The gas release, pH shift, and free radicals are nevertheless expected to be cytotoxic. More recent strategies that are compatible with cell encapsulation make use of sacrificial gel beads that degrade after gel injection [25,26]. As a result, the pores created have roughly spherical shape, with connectivity happening only when the concentration of the porogen is very high, and pore sizes in the hundreds of micrometers. The gels presented in this work, on the other hand, have pore sizes ranging from approximately 0.5 to 50 μm , and a thread-like, fully interconnected morphology, optimal for neurite or single cell infiltration rather than entry of large cellular clusters. Also, the pores created with our method form after injection, which makes the gels compatible with microneedle delivery and ensures local isotropy of the formed structures.

2. Results and discussion

2.1. Microstructuring of PEG hydrogels with polysaccharides

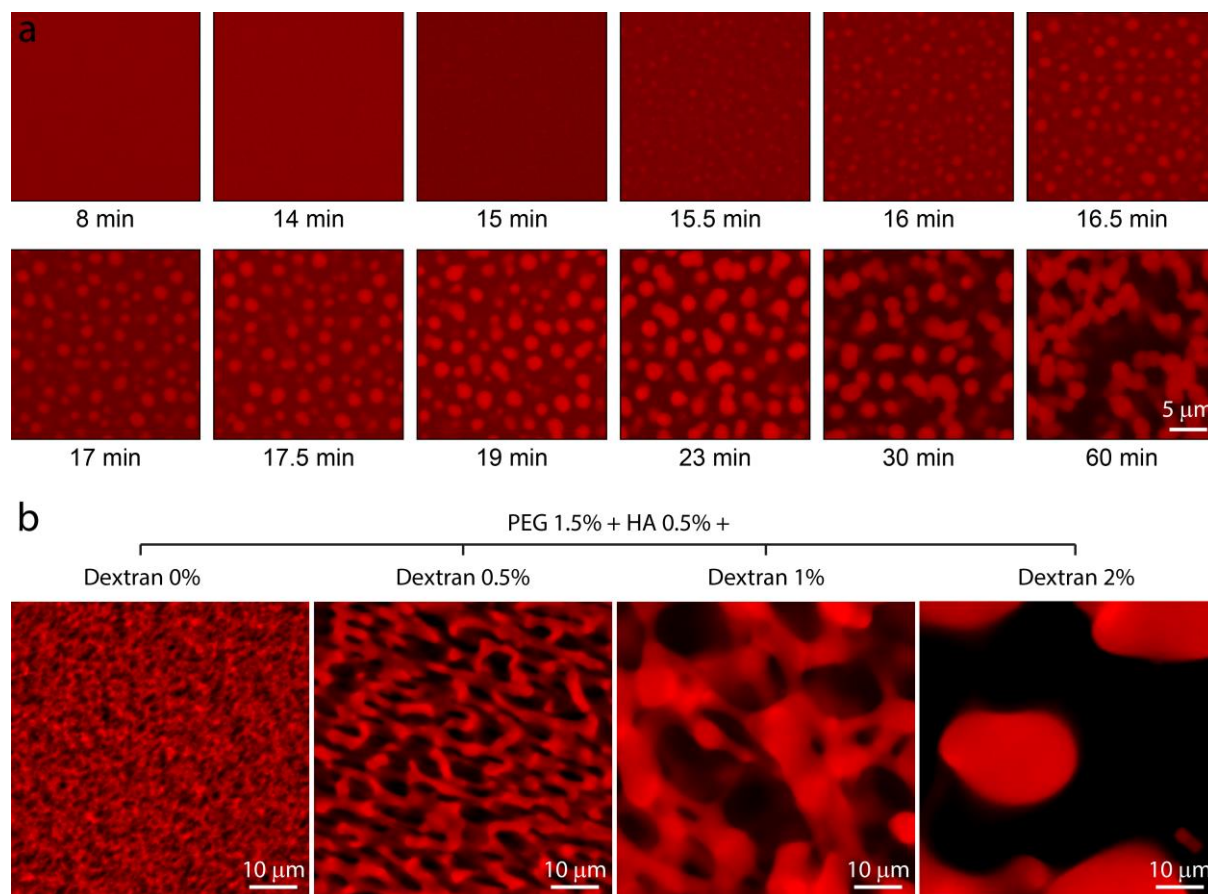


Figure 1 (grey in print, 2 columns). Macroporous PEG gel formation through PEG cross-linking in the presence of polysaccharides. (a) Monitoring of the phase separation during gelation. The sample is tetramethylrhodamine (TMR) tagged PEG 1.5% (w/v) gelled at room temperature (slower than the 37 °C used in the rest of the paper) in the presence of MA 2% (w/v) using PEG-dithiol as a cross-linker, imaged with confocal laser scanning microscopy (CLSM). Time post-mixing is indicated. Scale bar: 5 μm . (b) Demonstration of pore size control with a simple 3-component system: PEG is used as a cross-linked gel precursor, HA as a strong viscosity enhancer (and weak PEG-excluding component), and dextran as a strong PEG-excluding component. Variation of the dextran concentration from 0 to 2% (w/v) produces pores spanning two orders of magnitude (i.e. 0.5 to 50 μm).

PEG has been long known to form aqueous biphasic systems with dextran and some salts [27], due to its water organizing properties [28]. This physical effect has been used extensively for protein extractions [29], and shown to be useful for gel microsphere formation

[30], but its potential for in situ self-assembly of macroporous scaffolds has not yet been shown. This is probably because the phase separation typically proceeds through fast microsphere formation, with subsequent fusion and decantation, which doesn't provide percolating networks of pores and gel. In one occurrence, interconnected networks could be obtained by photocrosslinking overnight under tumbling the dextran of a high percentage PEG-dextran mixture [31]. Despite its merits, this method does not enable in situ gelling and cell encapsulation, and the resulting scaffolds have low transparency.

We found that the key to generate macroporous hydrogels in a way that is compatible with cell encapsulation and injection was to combine low polymer contents and high viscosities. The low polymer content guarantees that the PEG and polysaccharide solutions are initially miscible [32]. Then, since phase separation in aqueous systems is highly dependent on the molecular weight [33], phase separation is triggered by the PEG chain elongation that happens in the presence of the cross-linker (**Figure 1a**). The high viscosity prevents the phases from decanting and/or collapsing into microspheres before the structures are stabilized by gel formation.

The pore size is tunable by changing the nature and concentration of the polysaccharide. As an illustration of the versatility of the method, we show macroporous gels with pore sizes from 0.5 μm to more than 50 μm created by changing one parameter in a 3-component mixture (**Figure 1b**). These pore widths range from well below to well above the size of a mammalian cell, therefore spanning the entire range of microstructures relevant to cell culture applications. In this mix, 4arm-PEG-VS and PEG-dithiol are used as gel precursors, and the PEG concentration is the prime determinant of gel stiffness (**Figure 2d**). HA is used as a high viscous supplement generating only small pores and dextran is used to tune the strength of the phase separation, and hence the pore size.

Other polysaccharides can also produce similar effects to various extents, and addition of peptides can slightly affect the outcome. **Figure S1** shows the physical characterization of two particular implementations of this method investigated for cortical neuron cultures, which result in gels with radically different microstructures: 4arm-PEG-VS 1.5% (w/v) cross-linked with MMP-cleavable peptides (containing two cysteines providing thiols for cross-linking by Michael addition) with 70% (v/v) of MA 2% (w/v) or HA 0.5% (w/v) respectively (denoted PEG+MA and PEG+HA). The gelation is done in cell culture medium (Neurobasal+B27) supplemented with HEPES buffer pH7.4. The polysaccharides were chosen for being both chemically inert, available in high molecular weight to guarantee high viscosity at low concentration, and for having no (for MA) to little (for HA) specific biological effect. The concentrations of HA/MA stocks were adjusted to obtain similar complex viscosities over a large frequency range (**Figure 2b**), with static viscosities close to 1 Pa·s (similar to glycerol), which is high enough to prevent cell sedimentation and phase decantation, but still low enough to be pipetted/injected easily.

The advantage of starting from a homogeneous solution is that the final microstructure does not depend on the exact mixing or injection protocol, as long as the initial solution is well mixed: it is the basis for the formation of reproducible, homogeneous and isotropic pores. To quantify the pore size, connectivity and isotropy, we used a 4-arm-PEG-VS derivative with a fluorescent tag and confocal laser scanning microscopy (CLSM). PEG gels formed in the absence of polysaccharides appeared perfectly homogeneous (the distance between the PEG chains is estimated to be 5 to 50 nm [22] and the diffraction limit in our imaging

conditions is estimated to be 185 nm), whereas the PEG gels formed in the presence of HA or MA were macroporous (Figure S1a-c). 3D inspection revealed that the pores were fully interconnected (**Supplementary Video 1**). The autocorrelation function was computed (Figure S1e), and found to be isotropic. Pore size quantitation was done by fitting the data with the penetrable sphere model [34] (Figure S1f), yielding typical pore sizes of $0.82 \pm 0.1 \mu\text{m}$ for PEG+HA and $2.39 \pm 0.16 \mu\text{m}$ for PEG+MA. R^2 values were >0.98 , showing good agreement with the model. The pore volume fraction, $S_2(0)$, was found to be $58 \pm 4\%$ for PEG+MA and $43 \pm 1.6\%$ for PEG+HA (this last value should be taken with caution as the pores created in the presence of HA are close to the diffraction limit, and therefore appear blurry; the pores in PEG-MA on the other hand are well resolved). It is noteworthy that HA and MA solutions of same viscosity give rise to dramatically different porous structures: this is expected as phase separation kinetics are known to depend not only on viscosity but also on interfacial tension [29]. Pore size could also be adjusted by addition of variable amounts of dextran, which gives faster PEG exclusion without noticeably changing the viscosity, to yield pores of tunable size (data not shown).

The low polymer contents also guarantee small differences of density and optical index between both phases [35]. The former is interesting to avoid settling, which would result in differences between the pore size at the top and bottom of the gels. The latter avoids light diffraction within the gels which results in perfect gel transparency (**Figure S2**), something quite exceptional for macroporous scaffolds. This enables optical imaging over several millimeters of depth, and easy observation of cells with differential interference contrast (DIC).

Percolating macroporous gels, such as those described in this study, are of strong interest for tissue engineering applications as their open passageways maximize transport properties and enable fast neurite extension or cell invasion, depending on the pore size. Such large interconnected pores are typically found in natural fibrillar matrices like collagen and fibrin, but not in classical chemically cross-linked hydrogels, that have 5-50 nm pore size [22].

2.2. Physical characterization

An increase in viscosity gives slower diffusion and therefore slower gelation kinetics. But this effect is more than counterbalanced by the increase in concentration through volume exclusion, and as a result porous PEG gels were formed with enhanced kinetics. It is particularly interesting as this enabled the formation of gels with optimal kinetics at physiological pH, whereas similarly good gelling times are normally only achieved at pH 8.0 (Figure 2a/c), which is stressful for cells in general [22] and can result in damage or death for sensitive cells such as neurons. Definitions of gelling time and stiffness used in this work are given in the methods and illustrated in **Figure S3**.

PEG concentrations of 1.2 to 1.9% (w/v) gave access to a range of stiffness of the order of 100 Pa expected to be appropriate for neuronal cultures according to prior art [36] (Figure 2d).

Since encapsulated cells might sense the stiffness of the PEG phase pillars rather than the macroscopic stiffness that can be measured in bulk, we used a finite element model based

on CLSM images of a macroporous gel to estimate the ratio between the bulk stiffness and the PEG phase stiffness (**Figure S4**). We found the static modulus of the PEG phase to be approximately 3 times higher than the bulk static modulus. When the pore size is large compared to the cell size, as with MA structuring, one can expect the cells will sense this higher modulus rather than the bulk one. When the pore size is small compared to the cell size, as is the case with HA-structuring, one would expect that some averaging of the mechanical properties of the two phases already happens over a growth cone width, and that the cells feel a stiffness closer to the bulk one.

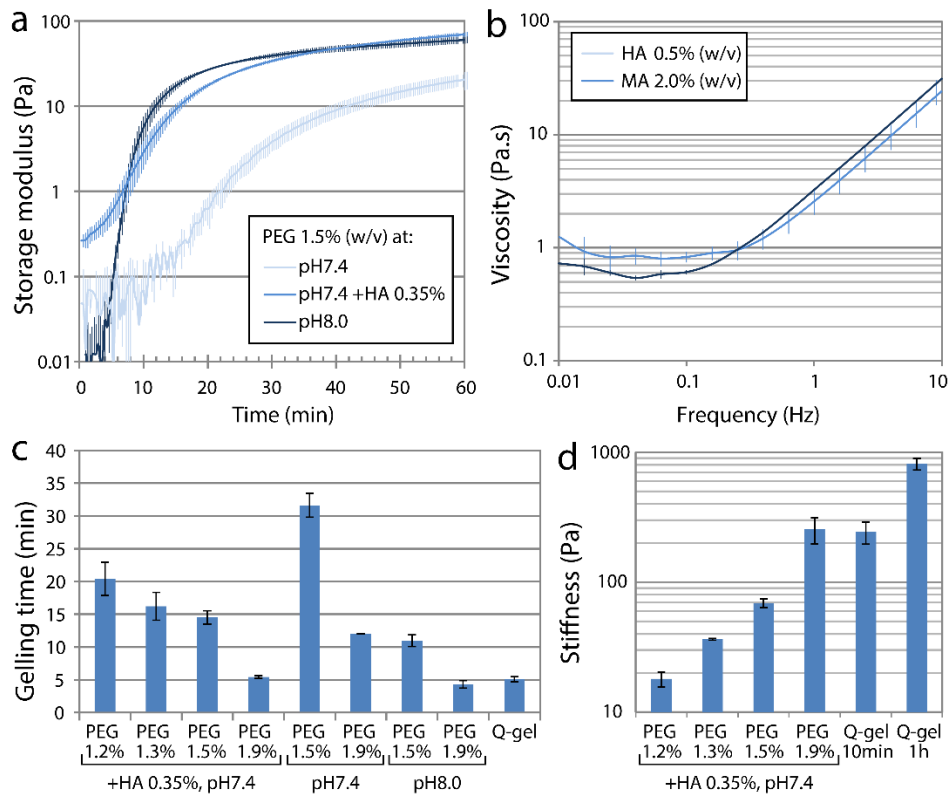


Figure 2 (grey in print, 1 or 1.5 columns). Volume exclusion enhances the kinetics of PEG gelation with Michael addition. (a) Rheologic monitoring of gelation. HA supplementation enable gels to form at physiological pH with nearly the same kinetics as obtained at pH8.0 with pure PEG gels. (b) Complex viscosity of stock solutions of HA and MA in complete growth medium at 37 °C. (c) Gelation time. Higher PEG content or pH result in faster gelation, as does replacing the gelation media by the viscous HA stock solution. Q-gel is given as a reference of a commercially-available PEG gel. (d) Stiffness after 60 min of gel formation (initial plateau). PEG concentrations between 1.2 and 1.9% (w/v) span a range of stiffness relevant to the developing nervous system, assumed to give best conditions for axonal growth. Q-gel stiffness is also shown after 10 min gelation, as it is the time at which the manufacturer recommends adding media. Error bars: SD (n=3).

Transport properties through the macroporous networks were also evaluated. Fluorescently-tagged neutravidin was chosen as a weakly interactive and average sized (60 kDa tetramer) model protein, and diffusion speeds were measured with the diffusion into stab method (**Figure S5**). Diffusion coefficients of $61 \pm 5 \mu\text{m}^2/\text{s}$ and $74 \pm 11 \mu\text{m}^2/\text{s}$ (SEM, n=5) were found in the classical and macroporous gels respectively, which showed no significant difference. These values also show no significant difference from the unhindered diffusion speed in water of $64 \mu\text{m}^2/\text{s}$ for avidin (an almost identical protein), measured by dynamic light scattering [37]. This shows that the low PEG concentrations used for neural tissue regeneration do not markedly affect protein diffusion speeds, and therefore that the macropores do not bring a transport improvement in this case. The situation might be very different if the macroporous gels are used for other tissues which are considerably stronger and hinder diffusion in the absence of pores.

On the other hand, we could observe strong differences in the equilibrium concentrations of various macromolecules in and out of the PEG phase. Even though the model protein could diffuse at full speed through the PEG, the concentration that could be reached in the PEG phase after equilibration was only 79% of the concentration in the supernatant and in the macropores. The situation was more extreme with larger biomolecules: the equilibrium concentration of chitosan in the PEG phase was 44% of that in the pores, and the concentration of 500 kDa dextran-FITC in the PEG was only 13% of the pore value (**Figure S6**). This shows that various biomacromolecules poorly enter PEG gels, because of thermodynamic rather than kinetic reasons, and that the presence of macropores enables these molecules to be accessible to encapsulated cells. This property could be critical when signaling from nano-particles like exosomes have to reach the cells, or when large matrix assemblies like collagen or aggrecan are deposited.

2.3. DRG encapsulation

DRGs are the most common in vitro model of peripheral axon regeneration and, as full explants, are easy to culture due to their resistance to chemical and biological stress. They are commonly grown in 2D to test the bioactivity of various substrates and in 3D in fibrin [38] or collagen [39], though these tend to degrade within a few days due to the high concentration of proteases around the explant [40]. We found that non-degradable porous PEG gels were permissive to peripheral axon invasion and stable for extended amounts of time (**Figure 3**). For this, DRG explants from E9.5 chick embryos were encapsulated in disks (4 mm x 1.5 mm) of PEG gel formed from 4arm-PEG-VS 0.8% (w/v), cross-linked with stoichiometric amount of PEG-dithiol in the presence of HA 0.525% (w/v) and dextran 1.4% (w/v). Whole gel imaging of the live cell processes (stained by calcein AM) after 30 days revealed that a dense mesh of axons was scattered through the entire gel, showing permissiveness as well as long-term stability. Cell death was obvious on the surface of the explant but not inside, as seen from the propidium iodide (PI, dead) / Calcein AM (live) staining pattern. This suggests that the outer cell layer helps to protect the inner cells from the stress associated with encapsulation.

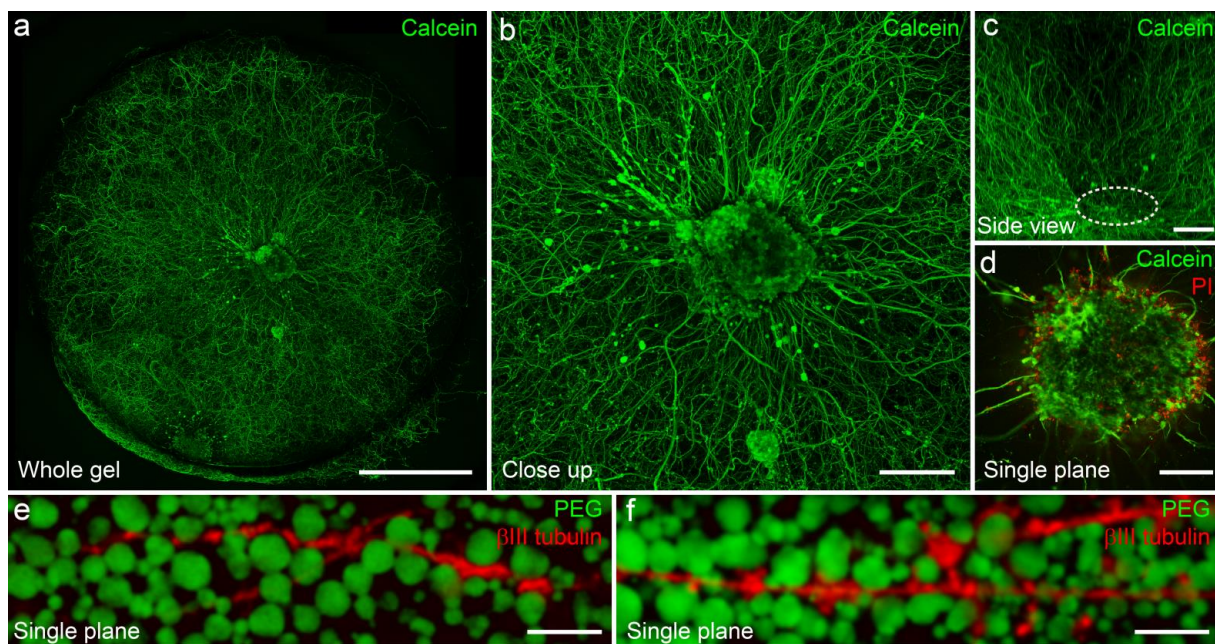


Figure 3 (color in print, 2 columns). Dorsal root ganglia (DRGs) in non-degradable macroporous PEG gels. (a) Whole gel imaging after 30 days of culture shows complete invasion by axons from the DRG (cluster in the center, fluorescence imaging 1.5 mm maximum intensity projection (MIP)). (b) Close-up of the center showing high neurite density (top view, 1.5 mm MIP). (c) Side view of (b) showing neurites are distributed through the whole depth of the gel (1.5 mm MIP). The DRG position is highlighted, as only its lower surface is visible, the rest of it and the neurites in a cone behind are less accessible to the light and appear dark. (d) Live/dead imaging of a cross-section of the DRG. A crown of dead cells is visible but the inner cells are alive. (e) Close up of axons extending through the pores one day after encapsulation and (f) 21 days after encapsulation, showing stability of the cross-linked PEG phase and permissiveness of the liquid-filled polysaccharide phase. Scale bars: 1 mm (a) 250 μm (b) 250 μm (c) 125 μm (d) 15 μm (e-f).

2.4. 3D neural networks from rat cortical neurons in porous PEG

Primary rat cortical neurons were encapsulated in macroporous gels formed with increasing amounts of HA (**Figure 4**). The neuron viability, rate of neurite outgrowth, and gel degradation were quantified, as they are the most critical parameters to optimize for 3D neural network formation. The commercial product Q-gel was used as a non-porous classical PEG gel control, as it represents the current gold standard and has been successfully used for the encapsulation of many cell types.

As neurons are known to grow best in very soft fibrin and collagen matrices, we chose a concentration of 1.5% (w/v) PEG, which has a storage modulus of 70 Pa just after gelling. Pilot experiments showed markedly reduced viability when using a non-cleavable cross-linker (**Figure S7**). In attempts to explain this, we found that tetramethyl rhodamine (TMR) tagged

4-arm-PEG-VS could be taken up by the neurons over the time of gel formation (**Figure S8**), which led us to hypothesize that neurons should be able to metabolize the gel fragments to prevent toxicity. We therefore used matrix metalloproteinase (MMP) cleavable peptides as cross-linkers.

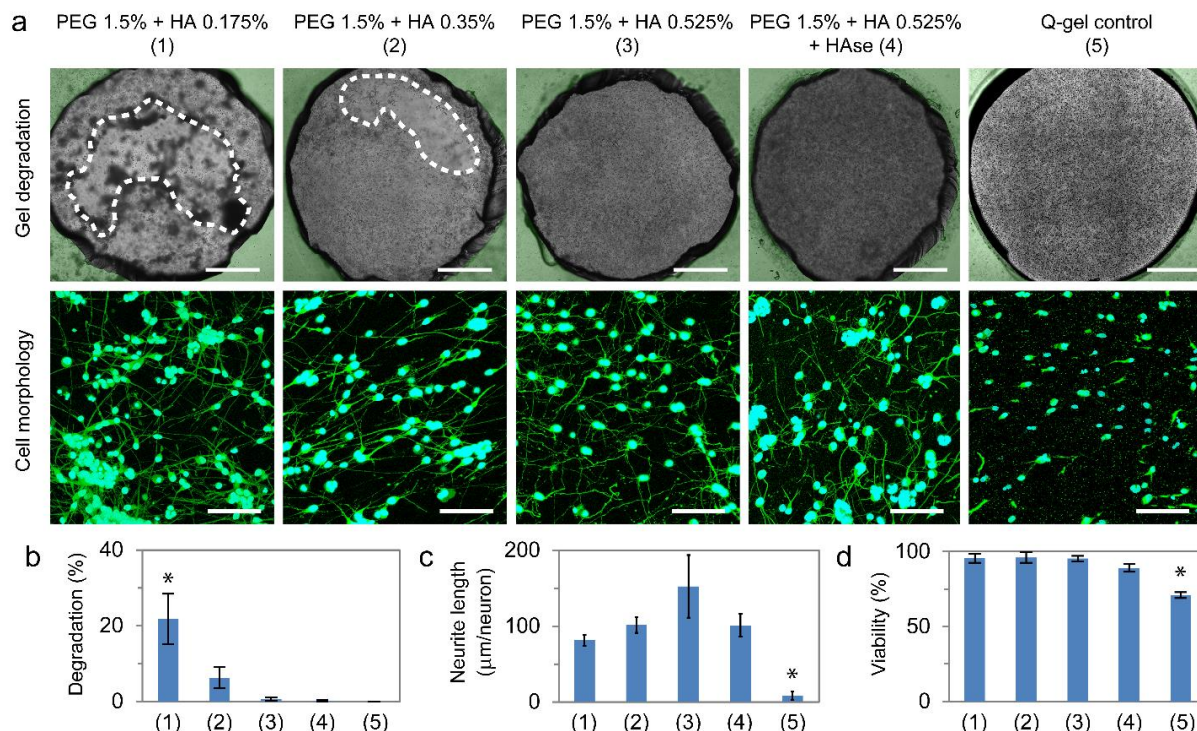


Figure 4 (grey in print, 2 columns). Microstructuring with HA improves the stability of soft gels and allows fast neurite outgrowth, gel formation at pH 7.4 and high viability. Hyaluronan can be removed after gelation without killing the neurons, degrading the gel or preventing the neurite outgrowth. (a) Macroscopic gel degradation as seen in brightfield at D2, with degraded parts highlighted in white and PDMS support in green, and close up of the morphology of the neurons as seen by CLSM (200 μ m MIP). PEG 1.5% gels formed without HA are not shown because they were not stable for 2 days and therefore could not be quantified. Staining is calcein/DAPI (1 to 3) and β III-tubulin/DAPI (4 and 5). Both methods stain all the neurites/cell bodies, but partially degraded gels did not withstand immunostaining, so the cell morphology was directly imaged on calcein stained live samples (Gamma adjusted for visualization of neurites without saturation of cell bodies). (b) Macroscopic degradation at D2 as percentage of the gel area. (c) Total neurite length divided by the number of cell bodies in a sample volume at D2. (d) Viability at D2. Error bars: SD ($n=6$ for degradation, $n=3$ for viability and neurite length). *: Different from all other conditions ($p<0.01$). Others are comparable ($p>0.01$). Scale bars: 1 mm (first line) and 25 μ m (second line).

The quantification two days after encapsulation (D2) showed that neurons retained very high viability (>95%) in the porous gels (Figure 4d), which is far better than the current

most successful synthetic neuron supporting gel, Puramatrix [41,42]. Viability in the Q-gel control was reduced to 70%, probably due to the short exposure to a higher pH as well as to the higher PEG content used in the classical approach. Neurite extension was ≈ 100 μm /neuron on average on D2, independent of the HA percentage (Figure 4c), which shows the low stiffness chosen is appropriate to support fast neurite extension. Microstructuring had a major influence on the stability of the gels: increasing amounts of HA resulted in less macroscopic degradation (Figure 4b). Gels formed with no HA were fully degraded within two days (which is why this condition is not in Figure 4), whereas gels formed with 0.525% (w/v) of HA were fully stable after more than a month. This is expected as in the macroporous gels, the PEG is excluded from roughly half of the volume, making the PEG concentration in the PEG phase approximately twice that of homogeneous PEG gels. These PEG pillars are separated by weak channels of uncrosslinked HA. This makes these microstructured gels more stable, while maintaining their potential to support fast neurite outgrowth.

As an additional characterization of how the mechanical properties evolve over the culture time, we measured the indentation modulus of microstructured gels after 2 and 21 days in culture, compared to day 0, and found an initial drop of 50% in the stiffness in the first two days (probably largely associated with the initial gel swelling), but a stable stiffness thereafter (**Figure S9a-b**).

Using well-defined, cell-free systems, we further investigated whether the increased stability was due to higher resistance to enzymatic degradation, or simply to increased physical stability of the denser PEG phase (Figure S9c-d). To test this, we used indentation testing to monitor the papain degradation of MMP-sensitive PEG gels and found both macroporous and classical gels degraded equally fast. On the other hand, when monitoring in mass the stability of PEG gels with various concentrations of PEG, we found the macroporous gels were markedly more stable for low polymer contents. The increased stability observed is therefore rather due to physical stability rather than to enzyme resistance.

Hydrogels microstructured with MA were tested as well for their ability to support cultures of dissociated cortical neurons. These gels had a large, open pore structure that resulted in misshapen cell morphology, as the cell bodies adapt their shape to the multi-micrometer sized pores in which they lie and neurites make sharp turns to follow them (**Figure S7, S10**). Since this morphology is not typically seen in vivo, we did not study this formulation further for this application. The sub-micrometer pores created by HA form instead a thin and dense network in which the cell bodies and neurites appear smooth, as they do in vivo.

Although it has long been assumed that laminin or laminin peptides are necessary for neurite outgrowth in 3D hydrogels [11,43], we demonstrate here excellent neurite outgrowth in PEG+HA microstructured gels in the absence of any adhesion cues. This is particularly noteworthy given PEG's stealth, anti-adhesive and non-interactive properties [14]. Several lines of data suggest that neurite extension mainly relies on physical properties. Firstly, we tested whether the HA provided important adhesion cues. For this, we digested it with 1 mg/ml hyaluronidase (Hase) immediately after gel formation, which resulted in HA removal (**Figure S11**). Neurite extension was not affected, which showed that HA was not needed for adhesion. Additionally, we noticed that when MA was selected for phase exclusion microstructuring, neurons still grew, although they lack receptors to this marine/bacterial polymer, further emphasizing that the presence of HA is not needed to support outgrowth.

Then, when PEG+HA and PEG+MA gels were covalently functionalized with IKVAV [44], even at high concentration, the neurite outgrowth was qualitatively similar to controls without IKVAV, whereas on 2D tissue culture plastic controls, the peptides potently induced neurite outgrowth in a concentration dependent manner (Figure S10). This shows that specific cues are not essential in the presence of an already optimal physical background. This is actually consistent with reports that the mechanism of action of IKVAV (which is the laminin fragment promoting the strongest neurite outgrowth as a 2D coating for central neurons) involves the formation of a soft and slightly adhesive surface through amyloid-like fibril formation. The mirror image peptide D-IKVAV, as well as mutated peptides still able to form fibrils, conserve this neurite outgrowth promoting activity, showing that even in 2D neurite outgrowth probably relies on physical properties of the substrate rather than specific recognition of the laminin domain [45,46].

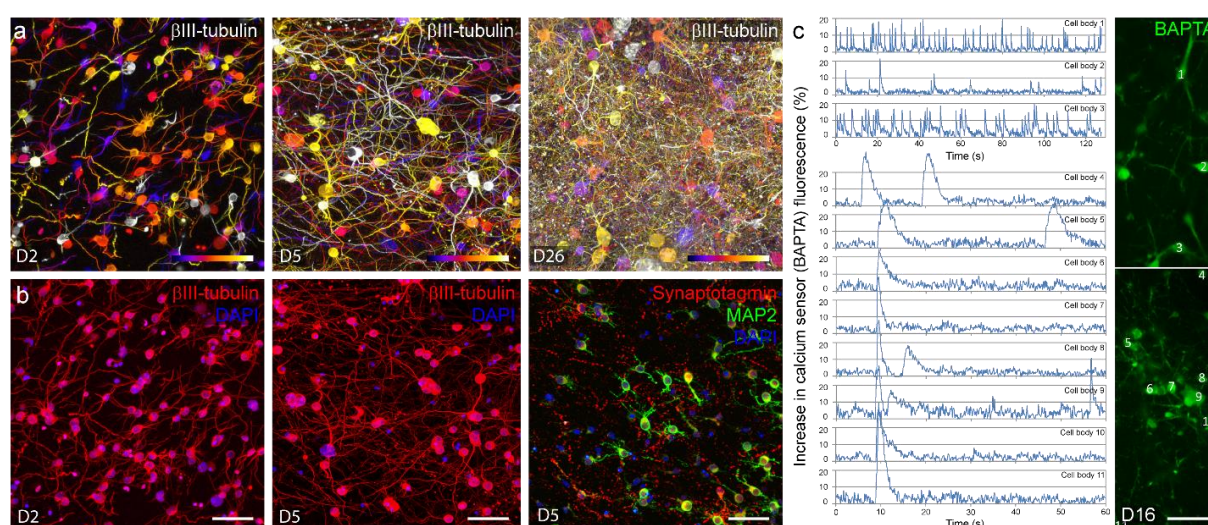


Figure 5 (color in print, 2 columns). Primary cortical neurons from E17 rat embryo encapsulated in porous PEG gels form long-term stable electrically active 3D neural networks. (a) 200 μm MIP with color-coded depth show that encapsulated neurons are homogeneously distributed and extend neurites in 3D through the matrix. Long neurites are already visible two days after encapsulation, and growth is continuing at increasing rate to form a dense network by D5. By D26, the whole gel is filled with a dense neurite network (Gamma adjusted for visualization of neurites without saturation of cell bodies). (b) Immunocytochemical markers (200 μm MIP from two-photon laser scanning microscopy stack acquisitions): $\beta\text{III-tubulin}$ is a neural marker that stains all neurites of embryonic neurons, synaptotagmin a marker of presynaptic terminals, and MAP2 a differentiated neuron marker known to stain only cell bodies and proximal neurites at this time point[47]. (c) Spiking activity in gels is observed with the intracellular calcium fluorescent reporter Oregon Green BAPTA-1. Independent spontaneous activity is observed (e.g. cell bodies 1 to 3) as well as synchronized activity (cell bodies 5 to 11 at 10 s), proving that a functional synaptically connected network was established by 16 days in the synthetic ECM. Scale bars: 100 μm with 200 μm color coded depth (a) and 50 μm (b,c).

It is also unlikely that neurons adhere non-specifically to proteins entrapped in the gel, as we work in serum free conditions and without growth factors. Initial neurite outgrowth also occurs too fast for matrix deposition by the cells to play a major role (typically, many $\sim 10\ \mu\text{m}$ neurites are visible one hour after encapsulation). Finally, we have ruled out non-selective adhesion to MMP-cleavable peptides: microstructured non-degradable PEG gels which are cross-linked with PEG-dithiol are completely free of amino acids or charges, and still as permissive to the neurite outgrowth, albeit with reduced viability (Figure S7). Overall, our data therefore indicates that physical properties rather than specific adhesion cues are of overwhelming importance to enable fast neurite extension in 3D.

Variations in macromer content from 1.2 to 1.9% (w/v) (18-250 Pa) did not significantly affect the neurite outgrowth over two or five days (**Figure S12**). The softest gels are more unstable, which can result in more damage and neurite loss. Non-porous controls at 1.5 and 1.9% (w/v), gelled at pH 8.0 without HA, were degraded after a few days. Q-gels were perfectly stable, but did not enable nearly as much neurite outgrowth as porous PEGs did.

In the optimized conditions, encapsulated primary neurons formed extensive networks within a few days, that increased in density and stayed stable for at least a month (**Figure 5a**). The main differentiated neuron markers were expressed similarly to what is known for 2D cultures (Figure 5b), and a large number of presynaptic densities were present. Solid spiking activity was observed after 16 days of culture using a fluorescent reporter of intracellular calcium. Furthermore, the activity was lost in the presence of the voltage gated sodium channel inhibitor tetrodotoxin, as well as with the glutamate receptor blockers CPP and CNQX, showing that calcium spikes are electrical in nature and triggered by glutamatergic excitation (**Figure S13**). Pre- and post-synaptic densities were omnipresent after 3 weeks of culture, including many densities in close apposition (**Figure S14**), and coordinated activity was clear (e.g. Figure 5c), which proves the formation of 3D networks with functional synaptic connectivity in the synthetic ECM.

2.5. Electrophysiology of 3D cultured mouse hippocampal neurons

To further investigate the functionality of the encapsulated neurons within the gel and to provide direct proof of their synaptic connectivity, we performed single and paired patch clamp recordings on mouse hippocampal neurons two weeks after embedding in the gel. We investigated cells with respect to their intrinsic properties, spontaneous action potential (AP) firing and post-synaptic potentials. Spontaneous postsynaptic potentials and action potential firing were found (**Figure 6a-b**), and the intrinsic properties of the cells such as membrane potential ($E_M = -65.5 \pm 2.7\ \text{mV}$, SEM $n = 14$), input resistance ($R_M = 479 \pm 102\ \text{M}\Omega$) and rheobase ($I_{\text{rheobase}} = 97.3 \pm 27.5\ \text{pA}$) indicated a physiologically healthy [48] state (Figure 6c). To validate the functional synaptic connections between neurons in the gel, we performed 4 paired patch clamp recordings (Figure 6d). In 3 cases, correlated excitatory post-synaptic potentials (EPSP) could be seen in cell B when eliciting action potentials in cell A by current injection (Figure 6e-f). Time delays between the action potential and the following post-synaptic potentials ranged from 1 to 1.5 ms, indicating monosynaptic connections (Figure 6g). Additionally, in some cases the overall frequency of post-synaptic potentials during

stimulation was increased, suggesting additional polysynaptic connectivity via other neurons in the network (Figure 6h). Overall, these electrophysiological measurements provide a direct confirmation of the neural network spontaneous spiking activity and 3D connectivity with quantitative electric potential and time information.

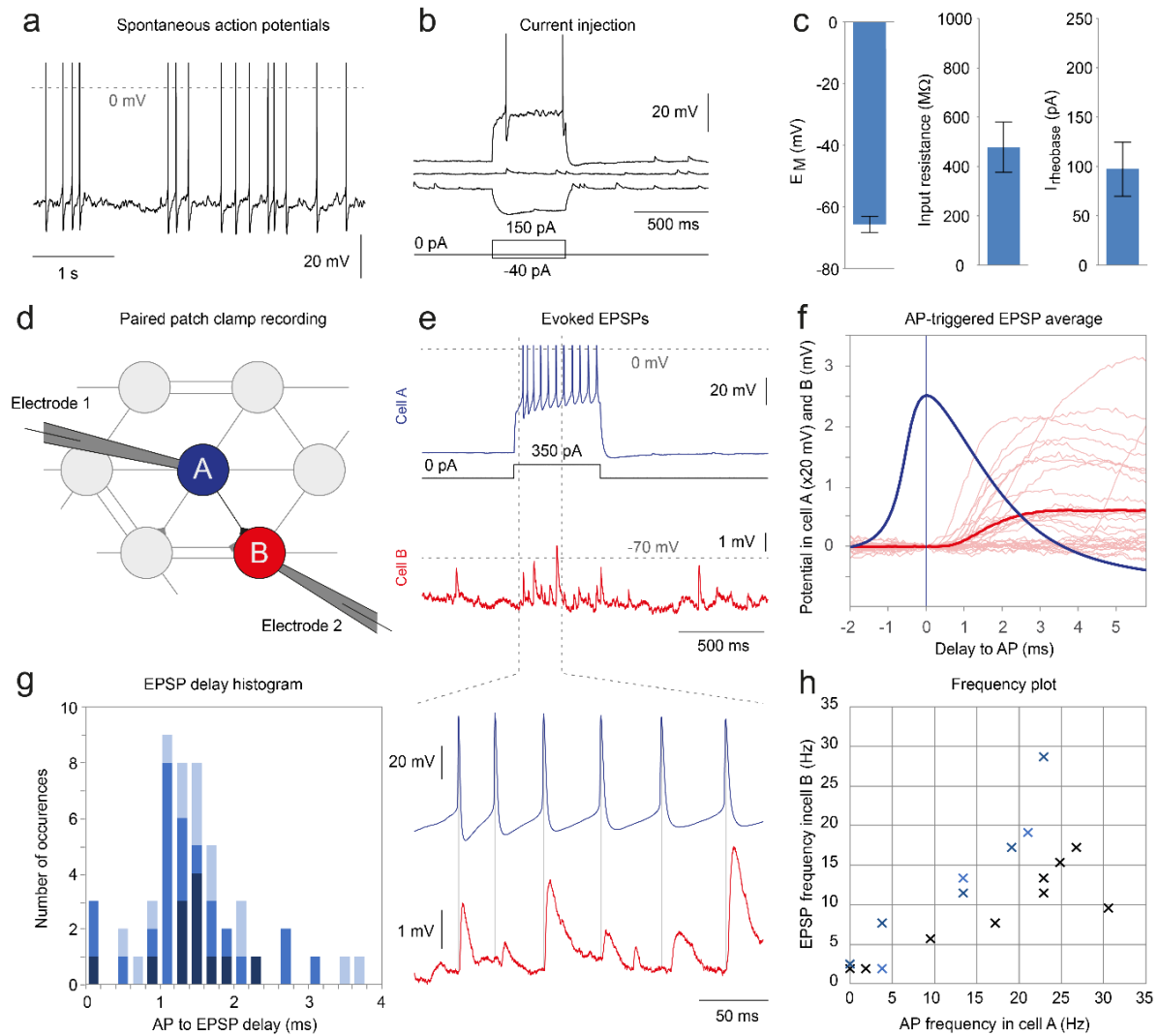


Figure 6 (grey in print, 1.5 or 2 columns). Electrophysiology of 3D cultured hippocampal neurons. **(a)** Example of passive single electrode recording showing spontaneous activity. **(b)** Representative current injection experiment showing elicited action potentials (APs). Note also the large number of spontaneous excitatory post synaptic potentials (EPSPs), showing the recorded cell is receiving synaptic input from other neurons. **(c)** Average intrinsic electrical properties of the neurons (error bars: SEM, n=14). **(d)** Dual patch clamp setup for assay of direct and indirect synaptic connections: cell B is recorded to monitor EPSPs while eliciting APs into cell A by current injection. **(e)** Example of recording from the dual patch clamp. Note the higher frequency of EPSPs in cell B during current injection in cell A, as well

as the synchronous APs-EPSPs in the close-up. (f) AP-triggered EPSP average (thick red line) overlaid with the single voltage recordings in cell B (thin red lines) and the average AP in cell A (thick blue line). Note the average potential in cell B is flat before the AP in cell A and increasing afterwards, confirming the EPSPs in cell B are linked to APs in cell A. (g) Quantitative measures of the delay between the peak of the AP and the peak in voltage increase in cell B evidence monosynaptic connections. (h) Correlation between AP frequency in cell A and EPSP frequency in cell B show the additional presence of polysynaptic connections.

2.6. In vivo sciatic nerve regeneration

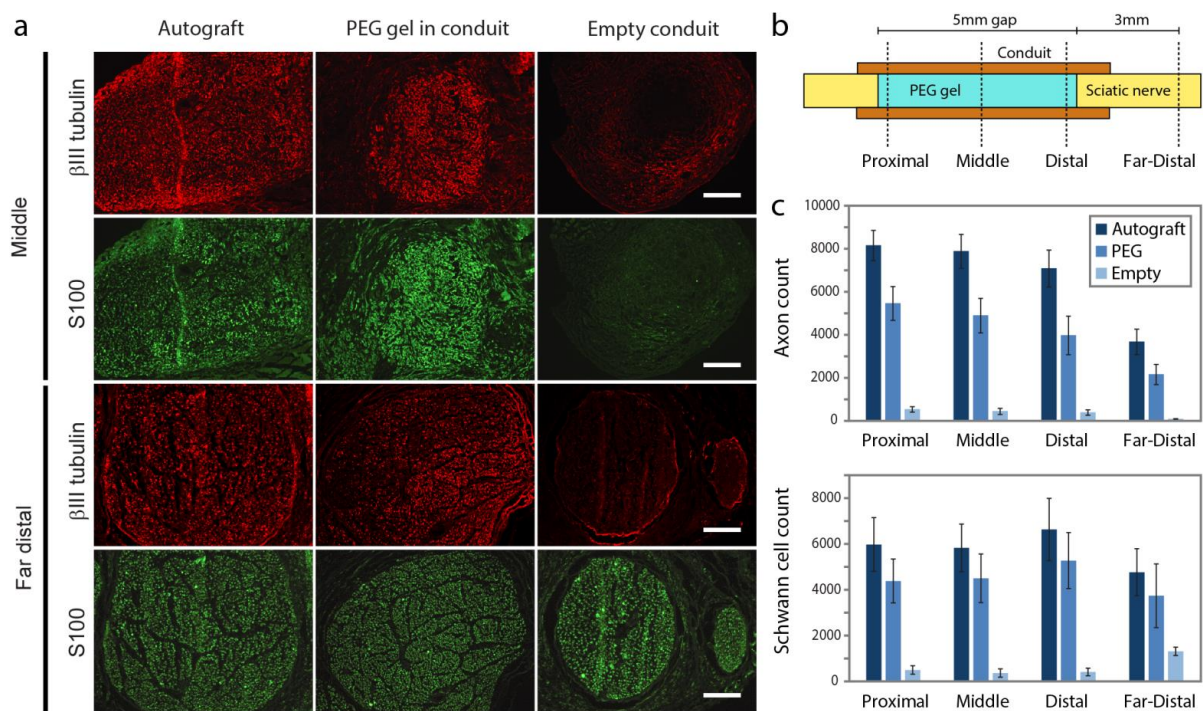


Figure 7 (grey in print, 2 columns). Sciatic nerve regeneration using macroporous PEG gels as filling for nerve guidance conduits. Autografts (gold standard) and empty conduit (control) are included for comparison. Analysis is done 4 weeks post-implantation. (a) Histology in transverse sections through the graft and distal nerve stump showing regenerating axons (βIII-tubulin) and Schwann cells (S100). Scale bars: 200 μm. (b) Schematics showing the conduit dimensions and quantification positions. (c) Axon and Schwann cell counts at different regeneration distances. Error bars are SD, n=6.

Given the promising in vitro results, we next investigated whether the macroporous gels would also be stable and permissive in vivo. The same gels that were used for in vitro 3D cultures of DRGs were gelled in collagen conduits and implanted into a 5 mm sciatic nerve gap in adult rats. Empty conduits were used as controls, and autografts were used as a gold

standard reference. The outcome was evaluated after 4 weeks, which is a time point at which axons are expected to have crossed the gap if the substrate is sufficiently supportive.

PEG gels were indeed found to be sufficiently stable and permissive to support axonal regeneration *in vivo*. The axon counts were around 70% of that found in the autograft at all levels in the graft and distal stump, whereas the counts in empty conduits were under 5% of the autograft counts (**Figure 7**).

In addition, as Schwann cells are known to provide a supportive environment to maintain axons and later on remyelinate them, we quantified S100+ cells and found the counts to be 80% of that in the autografts, showing very good invasion into the PEG. Empty conduits on the other hand contained very few Schwann cells. CD31+ cell counts (endothelial cells) in the middle of the PEG grafts were 60% of that in the autograft, whereas in empty conduits they were only at 25% of the autograft (**Figure S15**), showing the PEG filled conduit is also in the process of getting vascularized. Finally, ED1+ cell counts in the middle of the PEG gels and controls conduits were at 40% of the level in the middle of the autografts. This shows there is no accumulation of macrophages in the PEG gels of note, and by inference no immunogenicity or other pro-inflammatory effect of the material.

Since autografts are limited by donor site morbidity issues, the development of such synthetic hydrogels supporting axonal regeneration holds promise as a synthetic lumen filler of nerve conduits. The outcome here is interesting, since the gels did not include any supportive cells or growth factors, or even adhesion molecules like laminin or collagen, and are based on an inert synthetic material with optimized physical properties. In this form, the gels are particularly stable and easy to mass-produce, free from pathogen concerns (especially compared to the main alternative, fibrin pulled from human plasma). Further investigation will be needed to evaluate the potential of these scaffolds for clinical translation.

3. Conclusion

Many methods have been developed to create scaffolds with macroscopic or hierarchical porosity, typically by salt leaching, freeze-drying or electrospinning [49]. However these methods do not enable cell encapsulation or *in situ* formation. Here we present a unique method which allows direct encapsulation of cells into porous structures which are created by phase separation between PEG and high viscous polysaccharides as the PEG undergoes step growth polymerization. Defined 3D cultures enabling fast neurite outgrowth and synapse formation are of prime interest for studies relying on neuron-matrix interactions such as axonal guidance, growth cone machinery, synapse assembly and regeneration. The possibility to study the bioactivity of extracellular cues on a blank background is an important tool. Due to their perfect transparency, our microstructured gels are especially well suited for imaging studies.

Electrically active 3D models also represent a substantial improvement over 2D models. *In vitro* neural networks are an important tool for the study of electrophysiology, neuromodulation, neurotoxicology or for drug screenings. Their 3D counterparts have dramatically different connectivity, which yield data that is more relevant to the *in vivo*

situation. Network connectivity was recently studied on stacked 2D surfaces [50], however, our system goes one step further, by placing the neurons in a fully 3D environment.

The macroporous hydrogels described in this study provided an excellent mimic of the biophysical properties of the neural extracellular matrix, allowing for the first time formation of stable and functional neural networks in a synthetic PEG gel. For in vivo applications, it is of interest that the components and crosslinking chemistry used here are all biocompatible. In particular, PEG, HA and alginate are already used in the clinics. Due to the straightforward tunability of the system towards the micron range, one can also envision encapsulation of other cell types to control their migration, assembly and interactions in 3D space. In general, the combination of injectability, cyto- and biocompatibility, transparency, tunable pore size together with a simple self-assembling system based on commercial components is unprecedented. This makes macroporous hydrogels derived from aqueous dynamic phase separation a new fundamental tool interesting for a wide array of applications.

Supporting Information

Figures S1 to S15 and detailed protocols are available online or upon request to the authors.

Acknowledgements

We would like to thank Prof. J-M. Fritschy and Mrs. G. Bosshard for generously donating embryonic tissues, Prof. E. Stoeckli and Dr. B. Kunz for their valuable help with DRG isolation, and Prof. G. Skjåk-Bræk for kindly donating high viscous MA. This work was supported by the Swiss National Science Foundation ([CR32I3_166052](#) to MZW and 31003A_133076/1 to SM), FIFA/F-MARC, and CTI (16168.1 PFLS-LS to SM). The authors also acknowledge support of the Scientific Center for Optical and Electron Microscopy (ScopeM) of the ETHZ.

Data Availability Statement

The raw/processed data required to reproduce these findings is available upon request to the authors.

References

- [1] R. Mooney, B. Tawil, M. Mahoney, Specific fibrinogen and thrombin concentrations promote neuronal rather than glial growth when primary neural cells are seeded within plasma-derived fibrin gels., *Tissue Eng. Part A*. 16 (2010) 1607–19.
doi:10.1089/ten.TEA.2009.0372.
- [2] W. Ma, W. Fitzgerald, Q.Y. Liu, T.J. O’Shaughnessy, D. Maric, H.J. Lin, D.L. Alkon, J.L. Barker, CNS stem and progenitor cell differentiation into functional neuronal circuits in three-dimensional collagen gels, *Exp. Neurol.* 190 (2004) 276–288.

doi:10.1016/j.expneurol.2003.10.016.

- [3] M.C. LaPlaca, V.N. Vernekar, J.T. Shoemaker, D.K. Cullen, Three-Dimensional Neuronal Cultures, *Methods Bioeng. 3d Tissue Eng.* (2010) 187–204.
- [4] M.P. Lutolf, F.E. Weber, H.G. Schmoekel, J.C. Schense, T. Kohler, R. Müller, J. a Hubbell, Repair of bone defects using synthetic mimetics of collagenous extracellular matrices., *Nat. Biotechnol.* 21 (2003) 513–518. doi:10.1038/nbt818.
- [5] E. a Phelps, N. Landázuri, P.M. Thulé, W.R. Taylor, A.J. García, Bioartificial matrices for therapeutic vascularization., *Proc. Natl. Acad. Sci. U. S. A.* 107 (2010) 3323–3328. doi:10.1073/pnas.0905447107.
- [6] A. Mehanna, B. Mishra, N. Kurschat, C. Schulze, S. Bian, G. Loers, A. Irintchev, M. Schachner, Polysialic acid glycomimetics promote myelination and functional recovery after peripheral nerve injury in mice., *Brain.* 132 (2009) 1449–62. doi:10.1093/brain/awp128.
- [7] B. Demirbag, P.Y. Huri, G.T. Kose, A. Buyuksungur, V. Hasirci, Advanced cell therapies with and without scaffolds, *Biotechnol. J.* 6 (2011) 1437–1453. doi:10.1002/biot.201100261.
- [8] S.M. Willerth, S.E. Sakiyama-Elbert, Approaches to neural tissue engineering using scaffolds for drug delivery., *Adv. Drug Deliv. Rev.* 59 (2007) 325–38. doi:10.1016/j.addr.2007.03.014.
- [9] M.P. Lutolf, J.A. Hubbell, Synthetic biomaterials as instructive extracellular microenvironments for morphogenesis in tissue engineering., *Nat. Biotechnol.* 23 (2005) 47–55. doi:10.1038/nbt1055.
- [10] C.C. Lin, K.S. Anseth, PEG hydrogels for the controlled release of biomolecules in regenerative medicine, *Pharm. Res.* 26 (2009) 631–643. doi:10.1007/s11095-008-9801-2.
- [11] J.W. Gunn, S.D. Turner, B.K. Mann, Adhesive and mechanical properties of hydrogels influence neurite extension., *J. Biomed. Mater. Res. A.* 72 (2005) 91–7. doi:10.1002/jbm.a.30203.
- [12] N.A. Peppas, J.Z. Hilt, A. Khademhosseini, R. Langer, Hydrogels in Biology and Medicine: From Molecular Principles to Bionanotechnology, *Adv. Mater.* 18 (2006) 1345–1360. doi:10.1002/adma.200501612.
- [13] M.P. Lutolf, P.M. Gilbert, H.M. Blau, Designing materials to direct stem-cell fate., *Nature.* 462 (2009) 433–441. doi:10.1038/nature08602.
- [14] L.M.Y. Yu, N.D. Leipzig, M.S. Shoichet, Promoting neuron adhesion and growth, *Mater. Today.* 11 (2008) 36–43.
- [15] F.M. Veronese, Peptide and protein PEGylation: a review of problems and solutions., *Biomaterials.* 22 (2001) 405–17. <http://www.ncbi.nlm.nih.gov/pubmed/11214751>.
- [16] K.B. Bjugstad, K. Lampe, D.S. Kern, M. Mahoney, Biocompatibility of poly(ethylene glycol)-based hydrogels in the brain: an analysis of the glial response across space and time., *J. Biomed. Mater. Res. A.* 95 (2010) 79–91. doi:10.1002/jbm.a.32809.

- [17] K.B. Bjugstad, D.E. Redmond, K.J. Lampe, D.S. Kern, J.R. Sladek, M.J. Mahoney, Biocompatibility of PEG-based hydrogels in primate brain., *Cell Transplant.* 17 (2008) 409–15. <http://www.ncbi.nlm.nih.gov/pubmed/18522243>.
- [18] C. Papadimitriou, H. Celikkaya, M.I. Cosacak, V. Mashkaryan, L. Bray, P. Bhattarai, K. Brandt, H. Hollak, X. Chen, S. He, C.L. Antos, W. Lin, A.K. Thomas, A. Dahl, T. Kurth, J. Friedrichs, Y. Zhang, U. Freudenberg, C. Werner, C. Kizil, 3D Culture Method for Alzheimer’s Disease Modeling Reveals Interleukin-4 Rescues A β 42-Induced Loss of Human Neural Stem Cell Plasticity, *Dev. Cell.* 46 (2018) 85–101.e8. doi:10.1016/j.devcel.2018.06.005.
- [19] M.J. Mahoney, K.S. Anseth, Three-dimensional growth and function of neural tissue in degradable polyethylene glycol hydrogels., *Biomaterials.* 27 (2006) 2265–74. doi:10.1016/j.biomaterials.2005.11.007.
- [20] K.J. Lampe, R.G. Mooney, K.B. Bjugstad, M.J. Mahoney, Effect of macromer weight percent on neural cell growth in 2D and 3D nondegradable PEG hydrogel culture., *J. Biomed. Mater. Res. A.* 94 (2010) 1162–71. doi:10.1002/jbm.a.32787.
- [21] R.M. Namba, a a Cole, K.B. Bjugstad, M.J. Mahoney, Development of porous PEG hydrogels that enable efficient, uniform cell-seeding and permit early neural process extension., *Acta Biomater.* 5 (2009) 1884–97. doi:10.1016/j.actbio.2009.01.036.
- [22] G.P. Raeber, M.P. Lutolf, J.A. Hubbell, Molecularly engineered PEG hydrogels: a novel model system for proteolytically mediated cell migration., *Biophys. J.* 89 (2005) 1374–88. doi:10.1529/biophysj.104.050682.
- [23] D.D. McKinnon, A.M. Kloxin, K.S. Anseth, Synthetic hydrogel platform for three-dimensional culture of embryonic stem cell-derived motor neurons, *Biomater. Sci.* 1 (2013) 460. doi:10.1039/c3bm00166k.
- [24] E. Behraves, S. Jo, K. Zygourakis, A.G. Mikos, Synthesis of in Situ Cross-Linkable Macroporous Biodegradable Poly (propylene fumarate-co-ethylene glycol) Hydrogels, *Biomacromolecules.* 3 (2002) 374–381. doi:10.1021/bm010158r.
- [25] N. Huebsch, E. Lippens, K. Lee, M. Mehta, S.T. Koshy, M.C. Darnell, R. Desai, C.M. Madl, M. Xu, X. Zhao, O. Chaudhuri, C. Verbeke, W.S. Kim, K. Alim, A. Mammoto, D.E. Ingber, G.N. Duda, D.J. Mooney, Matrix Elasticity of Void-Forming Hydrogels Controls Matrix elasticity of void-forming hydrogels controls Transplanted Stem Cell-Mediated bone, *Nat. Mater.* 14 (2015) 1–19. doi:10.1038/NMAT4407.
- [26] L. Wang, S. Lu, J. Lam, F.K. Kasper, A.G. Mikos, Fabrication of cell-laden macroporous biodegradable hydrogels with tunable porosities and pore sizes., *Tissue Eng. Part C. Methods.* 21 (2015) 263–73. doi:10.1089/ten.TEC.2014.0224.
- [27] P.-Å. Albertsson, Partition of proteins in liquid polymer-polymer two-phase systems, *Nature.* 182 (1958) 709–711. doi:10.1038/182709a0.
- [28] B.Y. Zaslavsky, *Aqueous two-phase partitioning*, Marcel Dekker, 1995.
- [29] J. a. Asenjo, B. a. Andrews, Aqueous two-phase systems for protein separation: Phase separation and applications, *J. Chromatogr. A.* 1238 (2012) 1–10. doi:10.1016/j.chroma.2012.03.049.

- [30] D.L. Elbert, Liquid-liquid two-phase systems for the production of porous hydrogels and hydrogel microspheres for biomedical applications: A tutorial review, *Acta Biomater.* 7 (2011) 31–56. doi:10.1016/j.actbio.2010.07.028.
- [31] S.G. Lévesque, R.M. Lim, M.S. Shoichet, Macroporous interconnected dextran scaffolds of controlled porosity for tissue-engineering applications, *Biomaterials.* 26 (2005) 7436–7446. doi:10.1016/j.biomaterials.2005.05.054.
- [32] J. Ryden, P. Albertsson, Interfacial tension of dextran—polyethylene glycol—water two—phase systems, *J. Colloid Interface Sci.* 37 (1971) 219–222. doi:10.1016/0021-9797(71)90283-9.
- [33] D. Forciniti, C.K. Hall, M.-R. Kula, Influence of polymer molecular weight and concentration on phase composition in aqueous two-phase systems, *Fluid Phase Equilib.* 61 (1991) 243–262. doi:10.1021/jp2070858.
- [34] J.G. Berryman, Measurement of spatial correlation functions using image processing techniques, *J. Appl. Phys.* 57 (1985) 2374–2384. doi:10.1063/1.334346.
- [35] M. Mohsen-Nia, H. Modarress, H. Rasa, Measurement and modeling of density, kinematic viscosity, and refractive index for poly(ethylene glycol) aqueous solution at different temperatures, *J. Chem. Eng. Data.* 50 (2005) 1662–1666. doi:10.1021/je050130t.
- [36] G. Palazzolo, N. Broguiere, O. Cenciarelli, H. Dermutz, M. Zenobi-Wong, Ultrasoft Alginate Hydrogels Support Long-Term Three-Dimensional Functional Neuronal Networks, *Tissue Eng. Part A.* 21 (2015) 2177–2185. doi:10.1089/ten.tea.2014.0518.
- [37] M. Firnkes, D. Pedone, J. Knezevic, M. Döblinger, U. Rant, Electrically facilitated translocations of proteins through silicon nitride nanopores: Conjoint and competitive action of diffusion, electrophoresis, and electroosmosis, *Nano Lett.* 10 (2010) 2162–2167. doi:10.1021/nl100861c.
- [38] J.C. Schense, J. Bloch, P. Aebischer, J. a Hubbell, Enzymatic incorporation of bioactive peptides into fibrin matrices enhances neurite extension., *Nat. Biotechnol.* 18 (2000) 415–9. doi:10.1038/74473.
- [39] I. Allodi, M.-S. Guzmán-Lenis, J. Hernández, X. Navarro, E. Udina, In vitro comparison of motor and sensory neuron outgrowth in a 3D collagen matrix., *J. Neurosci. Methods.* 198 (2011) 53–61. doi:10.1016/j.jneumeth.2011.03.006.
- [40] S.M. Willerth, K.J. Arendas, D.I. Gottlieb, S.E. Sakiyama-Elbert, Optimization of fibrin scaffolds for differentiation of murine embryonic stem cells into neural lineage cells, *Biomaterials.* 27 (2006) 5990–6003. doi:10.1016/j.biomaterials.2006.07.036.
- [41] A. Kaneko, Y. Sankai, Long-Term Culture of Rat Hippocampal Neurons at Low Density in Serum-Free Medium: Combination of the Sandwich Culture Technique with the Three-Dimensional Nanofibrous Hydrogel PuraMatrix, *PLoS One.* 9 (2014) e102703. doi:10.1371/journal.pone.0102703.
- [42] A. Liedmann, A. Rolfs, M.J. Frech, Cultivation of Human Neural Progenitor Cells in a 3-dimensional Self-assembling Peptide Hydrogel, *J. Vis. Exp.* (2012) 1–7. doi:10.3791/3830.

- [43] J.P. Frampton, M.R. Hynd, M.L. Shuler, W. Shain, Fabrication and optimization of alginate hydrogel constructs for use in 3D neural cell culture., *Biomed. Mater.* 6 (2011) 015002. doi:10.1088/1748-6041/6/1/015002.
- [44] K. Tashiro, G.C. Sephel, B. Weeks, M. Sasaki, G.R. Martin, H.K. Kleinman, Y. Yamada, A synthetic peptide containing the IKVAV sequence from the A chain of laminin mediates cell attachment, migration, and neurite outgrowth., *J. Biol. Chem.* 264 (1989) 16174–82. <http://www.ncbi.nlm.nih.gov/pubmed/2777785>.
- [45] M. Yamada, Y. Kadoya, S. Kasai, K. Kato, Ile-Lys-Val-Ala-Val (IKVAV)-containing laminin α 1 chain peptides form amyloid-like fibrils, *FEBS Lett.* 530 (2002) 48–52. <http://www.sciencedirect.com/science/article/pii/S0014579302033938> (accessed September 17, 2014).
- [46] M. Nomizu, A. Utani, N. Shiraishig, M.C. Kibbey, Y. Yamada, P.P.R. T, The all-D-configuration segment containing the IKVAV sequence of laminin A chain has similar activities to the all-L-peptide in vitro and in vivo, *J. Biol. Chem.* 267 (1992) 14118–14121.
- [47] K.S. Kosik, E. a Finch, MAP2 and tau segregate into dendritic and axonal domains after the elaboration of morphologically distinct neurites: an immunocytochemical study of cultured rat cerebrum., *J. Neurosci.* 7 (1987) 3142–3153.
- [48] G. Milior, M.A. Di Castro, L.P. Sciarria, S. Garofalo, I. Branchi, D. Ragozzino, C. Limatola, L. Maggi, Electrophysiological Properties of CA1 Pyramidal Neurons along the Longitudinal Axis of the Mouse Hippocampus, *Sci. Rep.* 6 (2016) 1–9. doi:10.1038/srep38242.
- [49] N. Annabi, J.W. Nichol, X. Zhong, C. Ji, S. Koshy, A. Khademhosseini, F. Dehghani, Controlling the porosity and microarchitecture of hydrogels for tissue engineering., *Tissue Eng. Part B. Rev.* 16 (2010) 371–83. doi:10.1089/ten.TEB.2009.0639.
- [50] M. Frega, M. Tedesco, P. Massobrio, M. Pesce, S. Martinoia, Network dynamics of 3D engineered neuronal cultures: a new experimental model for in-vitro electrophysiology., *Sci. Rep.* 4 (2014) 5489. doi:10.1038/srep05489.